Superplastic compressive flow in MgB$_2$

John D. DeFouw *, David C. Dunand

Department of Materials Science and Engineering, Northwestern University, Evanston, IL 60208, USA

Abstract

Macroplasticity in the brittle, superconducting ceramic MgB$_2$ would allow for the mechanical drawing of thin, dense superconducting wires, as done for metallic superconductors. Here, we report very large uniaxial compressive deformation (engineering strain of 67% or true strain of -1.1) without fracture at 1000 °C for specimens densified from commercially available MgB$_2$ powders with MgO and MgB$_4$ second phases. Plastic flow occurs under a diffusion-controlled mechanism with activation energies of 255–447 kJ mol^{-1} and stress exponents of 1.4–2.0, indicative of superplastic behavior.

© 2009 Acta Materialia Inc. Published by Elsevier Ltd. All rights reserved.

Keywords: Magnesium diboride; Superconductors; Superplasticity; Superplastic forming; Creep

1. Introduction

Since the discovery that MgB$_2$ is superconductive with a high critical temperature ($T_c = 39$ K) [1] without weak-link behavior at grain boundaries [2], rapid progress has been achieved in the fabrication of continuous MgB$_2$ wires by the powder-in-tube (PIT) method [3–8]. The in situ PIT process involves combining Mg and B powders within a metal tube, deforming the filled tube at low temperature into a wire, and reacting the powders at elevated temperature to form MgB$_2$. The ex situ PIT process draws a metal tube containing pre-reacted MgB$_2$ powders into a wire. In both cases, significant MgB$_2$ core porosity exists [6,7,9], because of incomplete powder densification and differences of molar volumes between reactants and product. The critical superconducting current density of the wire is greatly reduced by the porosity, while the flux pinning is also reduced at higher fields because of lack of grain connectivity [9–12]. While MgB$_2$ is a brittle ceramic at ambient temperature, macroplasticity at elevated temperature would allow for the mechanical drawing of thin, dense supercon-

ducting wires, as done for ductile metallic superconductors with lower T_c [13].

As for other hard, brittle ceramic powders, MgB$_2$ powders can be densified into dense bodies under near-hydrostatic conditions at elevated temperature by a combination of surface and volume diffusion, and microplasticity. MgB$_2$ powders have been densified by hot isostatic pressing (HIP) at 950–1000 °C with pressures of 100–200 MPa for 3–4 h [14–16], by uniaxial die hot pressing at 700 °C and 640 MPa for 10–90 min [17], by die upsetting at 800–900 °C under a maximum stress of 450 MPa [18], and by cubic anvil pressing at 800–1000 °C under ∼3 GPa [19,20]. These batch processes are, however, not amenable to continuous wire production. The continuous hot drawing or extrusion of pore-free MgB$_2$ wires, with or without a metallic sheath, would be highly desirable. However, wire drawing requires macroplasticity in MgB$_2$, which is much more difficult to attain than microplasticity under hydrostatic conditions (i.e. the HIP or die-pressing powder densification reviewed above) because fracture often occurs before the activation of the plastic deformation mechanism operating at high temperature, e.g. creep mediated by dislocations or vacancies. Borides, in particular AlB$_2$-type borides such as MgB$_2$, are difficult to sinter and deform due to their strong covalent bonding and high

---

* Corresponding author. Tel.: +1 847 467 3996.
  E-mail address: jdefouw@u.northwestern.edu (J.D. DeFouw).

Peierls stress [21]: only modest levels of compressive macro-plasticity have been reported at elevated temperatures for TiB$_2$ [22] and ZrB$_2$ [23,24].

Other brittle superconducting materials have been found to exhibit plasticity. For instance, the A15 structured intermetallic superconductors Nb$_3$Sn [25,26] and V$_3$Ga [27] undergo a transition from brittle to ductile at temperatures above 1400 and 1000 °C, respectively. In these compounds, a reduction in grain size reduces the brittle to ductile transition temperature but increases the flow stress required for deformation due to Hall–Petch strengthening [25]. In contrast, many copper oxide superconductors achieve high degrees of plastic deformation at high temperature as reviewed in Ref. [28]; these oxides include YBa$_2$Cu$_3$O$_{7-x}$ [29–33] Bi$_2$Sr$_2$CaCu$_2$O$_x$ [34] and TlBa$_2$Ca$_2$Cu$_3$O$_x$ [35], with grain refinement (<1 μm) enhancing the deformation to superplastic levels in YBa$_2$Cu$_3$O$_{7-x}$ [30–33]. To our knowledge, the high-temperature mechanical properties of MgB$_2$ have never been studied, probably because near-brittle behavior is expected as for other diborides, and because decomposition by Mg evaporation is difficult to prevent. Macroplasticity in MgB$_2$ would allow for continuous drawing of dense wire and other complex shapes without using an expensive batch processes such as HIP, and would also permit winding of sheathed wires into magnet coils without fracturing their MgB$_2$ core.

In this work, the high-temperature mechanical properties of MgB$_2$ are measured in uniaxial compression and tension at constant strain rates. Unexpectedly, the flow stresses for plastic deformation of MgB$_2$ are modest at temperatures (900–1000 °C) that are sufficiently low for easy processing, and a very high compressive true strain (>−1.0) can be achieved without fracture. These properties – which are very unusual for a covalent ceramic such as MgB$_2$ – may enable improved and simplified processes for fabricating continuous wires and devices from superconducting MgB$_2$.

2. Materials and methods

Two batches of commercial MgB$_2$ powder (99% purity, both purchased in 2001 from Alfa Aesar, Ward Hill, PA, with particle size below 44 μm) were packed into carbon-steel tubes (9.5 mm OD, 6.2 mm ID) and welded shut under vacuum. Batch A was HIP densified (Ultraclad Corp., Andover, MA) by first heating to 780 °C under 150 MPa gas pressure for 1.5 h and to 1065 °C under 150 MPa for 4 h, followed by furnace cooling. Batch B was HIP densified under 100 MPa for 4 h at 1065 °C, followed by furnace cooling. Cylindrical or rectangular specimens, ~3 mm in diameter/width and ~6 mm in height, were machined from the center of the densified billets A and B (avoiding the limited reaction layer near the steel tube wall) using a combination of electrodischarge machining and mechanical grinding. The compressive specimens were placed within a 19 mm ID tungsten carbide sleeve with tight-fitting tungsten carbide top and bottom pistons.

A small quantity of Mg powder (99%, Fisher Scientific, 200–400 μm) was placed within the sleeve around the specimen, where it melted and provided an Mg atmosphere during high-temperature experiments, thus preventing MgB$_2$ decomposition to MgB$_4$ and MgB$_7$. A compressive force was applied by an universal testing machine to the pistons of the assembly under static Ar atmosphere, with displacement rates ranging from 0.05 to 5 μm s^{-1}, corresponding to initial strain rates of 9×10^{-6} and 9×10^{-4} s^{-1}. Typically, three increasing rates were applied consecutively on a single specimen at each temperature. Also, two specimens were deformed at single average strain rates of 95×10^{-5} and 4×10^{-5} s^{-1} at 1000 °C up to compressive engineering strains of 41 and 67% (true strains of −0.57 and −1.1), respectively.

Tensile specimens were created from billet B, which was cut into 40 mm long cylindrical segments whose ends were machined into threads within the steel tube. These were then masked with tape while the center of the steel tube was dissolved by applying a 5 V potential in a saturated aqueous NaCl/20% CH$_3$COOH solution. The exposed MgB$_2$ central section was then mechanically ground to a 3 mm diameter and 12 mm gauge length. Two such tensile specimens were tested at strain rates of 1 and 2×10^{-5} s^{-1} at 1000 °C, with a baffle system to maintain Mg vapor near the sample and a static Ar atmosphere in the chamber.

Metallographic specimens were mechanically ground and polished to be imaged with a Hitachi S4800 scanning electron microscope. As-received powders, as-HIP-densified specimens and specimens deformed at 1000 °C were analyzed by X-ray diffraction (XRD) using a Rigaku D/MAX-IA diffractometer ($\lambda = 0.154$ nm) with 0.02° angular steps and 3 s dwell time, followed by Rietvelt refinement analysis to determine volume fraction of the phases present (MgB$_2$, MgB$_4$, MgO) as well as MgB$_2$ grain size.

3. Results and discussion

3.1. Microstructure

All specimens exhibit a dense microstructure, with a few small pores as observed through optical microscopy, and a bulk density of 2.60–2.66 g cm^{-3} determined from specimen dimensions. Their density is very near the theoretical density of 2.62 g cm^{-3} for MgB$_2$ [36] and likely varied from the theoretical value due to the presence of MgB$_4$ ($\rho = 2.48$ g cm^{-3}) and MgO ($\rho = 3.58$ g cm^{-3}) phases typical for these commercial powders [10,37]. These phases were identified by scanning electron microscopy (SEM) imaging and XRD, as shown in Fig. 1. The MgB$_2$ matrix contains 1–10 μm wide MgB$_4$ regions and 10–500 nm MgO particles. Rietveld refinement analysis of XRD patterns from as-received powders determined initial MgB$_2$ grain sizes of 62 ± 9 nm for powder A and 85 ± 8 nm for powder B, in general agreement with a value of 19 nm reported for the crystallite size of commercial MgB$_2$ powders consisting of 60 μm agglomerates of submicron
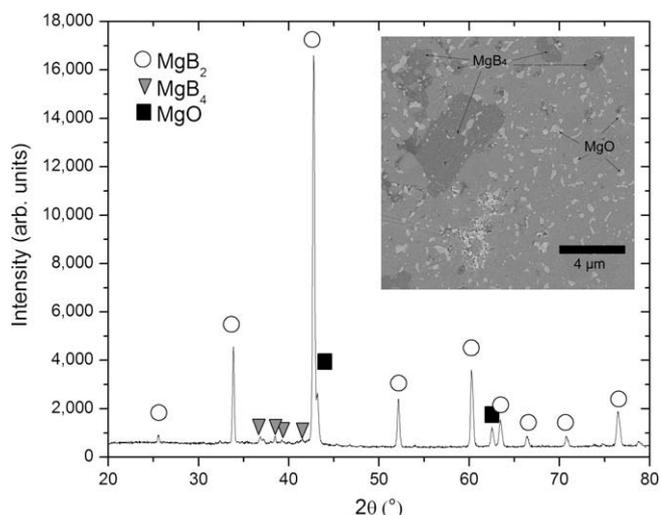
Fig. 1. XRD pattern for as-densified specimen A, identifying MgB_2 as the main phase and MgB_4 and MgO as minor phases. These phases are also visible with backscattered scanning electron microscopy (inset).

particles [10]. Rietveld analysis also provided an MgO volume fraction of ~3% for both batches, and MgB_4 volume fractions of ~5% for powder A and ~12% for powder B. The MgB_4 content, rather than grain size or HIP procedure, thus distinguishes the two types of powders.

3.2. Compressive superplastic deformation

Large-scale, superplastic-like deformation was demonstrated at 1000 °C at a constant strain rate of 4×10^{-5} s^{-1} in a specimen of sample B deformed to a compressive engineering strain of 67% (all strain values are uniaxial in the following), corresponding to a true strain of −1.1. As illustrated in Fig. 2, the experiment was interrupted four times to image the specimen (individual stress–strain curves are reported in Fig. 3), which showed near-uniform plastic compression without fracture or cracking. Another constant-rate experiment, with the stress–strain curve shown in Fig. 4, was carried out on a specimen of sample A at a much higher strain rate of 9.5×10^{-4} s^{-1} (5.7% min^{-1}), and terminated without failure after an engineering compressive strain of 41% (true strain of −0.57) had been accumulated. To our knowledge, no borides, and very few covalent compounds, exhibit such

Fig. 2. Photographs of a specimen of sample B deformed to an engineering compressive strain of 67% (true strain of −1.1) in four stages at 1000 °C without any cracking. Initial and final MgB_2 specimen heights are 6.0 and 2.0 mm. Initial strain rate for each stage was maintained at 4×10^{-5} s^{-1}.
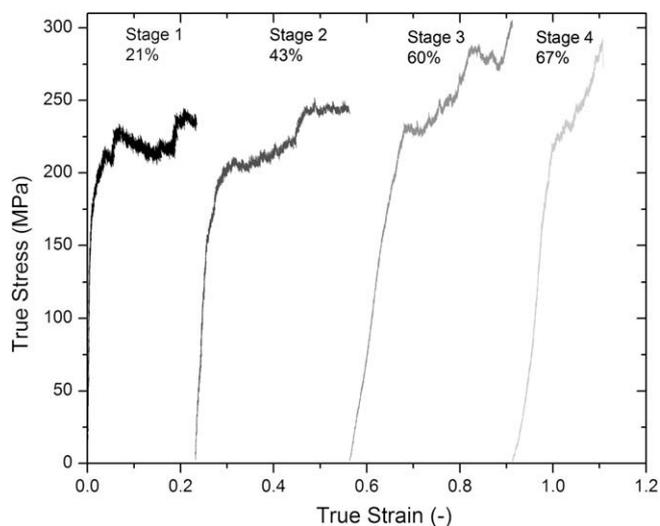

Fig. 3. Compressive stress–strain curves for a specimen of sample B deformed in four stages to 67% compression (true strain −1.1) at a strain rate of 4×10^{-5} s^{-1}. Photographs of the specimen at the end of each stage are shown in Fig. 2.
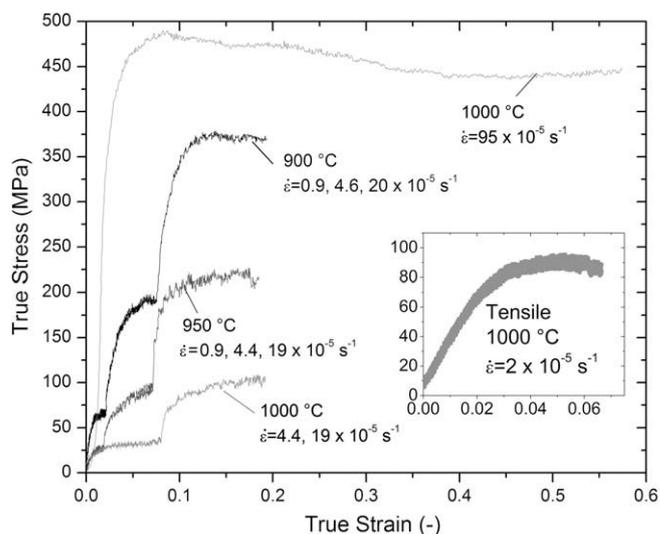

Fig. 4. Compressive stress–strain curves for specimens of sample A tested at 900, 950 and 1000 °C at constant strain rates varying between 0.9 and 95×10^{-5} s^{-1}. Inset shows a tensile stress–strain curve of a specimen of sample B.

a high degree of macroplasticity, especially when densified from commercial powders without chemical modifications or thermomechanical treatment to control grain size. Most ceramics show compressive ductility of a few percents at elevated temperature ($T/T_m > 0.7$, where T_m is the melting point), but very few exhibit the large-scale ductility (>20%) typical of metals and necessary for wire drawing. In rare cases, ceramics can exhibit superplasticity (tensile elongation in excess of ~100% [38]) at high temperatures – e.g. Y_2O_3-stabilized ZrO_2 (800% [39]), Al_2O_3 (65% [40]), hydroxyapatite (150% [41]), Si_3N_4 (230% [42]) and SiC (140% [43]) – when engineered to have stable, submicrometer grain sizes or when a high-temperature liquid phase is

present at the grain boundaries. Similarly engineered materials such as Al_2O_3 [44], Si_3N_4 [45] and SiC [46] can also exhibit superplasticity in compression (this term is reserved for tensile deformation in metals but is often used for compressive deformation of ceramics), but there is no literature report, to our knowledge, of superplastic borides.

A series of uniaxial compressive creep tests were performed on specimens of sample A without fracture between 900 and 1000 °C, with average flow stresses ranging from 27 to 454 MPa for strain rates between 9×10^{-6} and $9.5 \times 10^{-4} \, s^{-1}$, as shown in Fig. 4. Specimens of sample B exhibited similar compressive stress–strain curves (Fig. 5), but at somewhat higher flow stresses of 65–794 MPa for the same range of temperatures and strain rates. A rise in creep flow stress can be explained by an increase in grain size [38], but the 115 ± 15 nm grain size for as-densified billet B was in fact smaller than the 204 ± 47 nm grain size for as-densified billet A. Grain sizes remained substantially unchanged, within error, for both specimens A (157 ± 28 nm after testing for 10 min at 1000 °C) and B (156 ± 27 nm after testing for 11 h at 1000 °C). Rather, the higher flow stresses for specimens of sample B can be attributed to composite strengthening, due to the larger volume fraction of MgB_4 which is assumed to be more creep-resistant than MgB_2 and thus acted as reinforcement. The MgO fractions of both as-HIP specimen groups were ∼3% as with the as-received powders; the MgO and MgB_4 fractions increased to ∼7% and ∼15%, respectively, for both specimens A and B, after testing at high temperature.

3.3. Deformation mechanisms

By plotting the strain rate $\dot{\varepsilon}$ against the flow stress σ in a double-logarithm graph for the three test temperatures, as shown in Fig. 6, the creep data for specimens A and B can be fitted to the power-law creep equation:

$$\dot{\varepsilon} = A\sigma^n \exp\left(\frac{-Q}{RT}\right) \tag{1}$$

where Q is the activation energy, R the gas constant, T the temperature, A a constant and n the stress exponent. Best-fit parameters for specimens A are $n = 1.4$ and $Q = 255 \, kJ \, mol^{-1}$. A stress exponent near unity is typical of diffusional creep [38] and has been found for compressive creep of ZrB_2 ($n = 0.6$–1.7 at 1500–1600 °C) [24], Si_3N_4 ($n = 1$–2 at 1450–1650 °C) [45] and SiC ($n = 1.5$–1.7 at 1650–1700 °C) [46]. Stress exponents higher than unity may be indicative of an additional creep mechanism such as cavitation or a change in grain size [45], but an exponent up to $n = 2$ is adequate (but not sufficient) for large-scale superplastic deformation [38]. The creep activation energy measured here for specimen A (255 kJ mol^{-1}) is within the broad range of activation energies for interdiffusion measured during the $Mg + 2B = MgB_2$ synthesis within a similar temperature range (140 kJ mol^{-1} for B powders reacted at 670–900 °C [47] and 360 kJ mol^{-1} for B fibers reacted at 700–1000 °C [48]). This fact, together with the low stress exponent near unity, suggest that diffusional creep is the operating deformation mechanism for MgB_2, as observed for many ceramics with fine grains at a homologous temperature $T/T_m > 0.5$. The melting point of MgB_2 is not known since the compound decomposes to MgB_4 and MgB_7 at 900 °C under vacuum [49–51] and oxidizes in air, but it can be assumed to be similar to that of CrB_2 ($T_m = 2473$ K) or MnB_2 ($T_m = 2261$ K) with similar free energies of formation. As shown in Fig. 7, there is a linear correlation between melting point and Gibbs free energy of formation for nine isostructural AlB_2-type diborides (data from Ref. [50]). The best-fit line predicts a melting point of 2307 K for MgB_2, using its measured free energy of for-
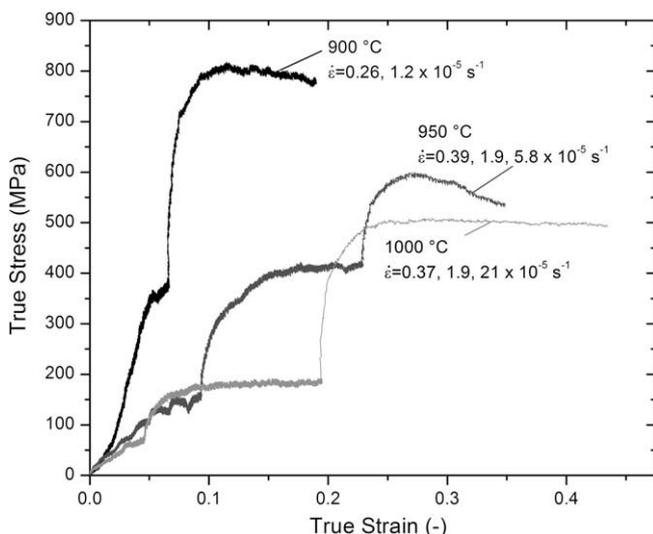
Fig. 5. Compressive stress–strain curves for specimens of sample B tested at 900, 950 and 1000 °C at constant strain rates from 0.26 to $21 \times 10^{-5} \, s^{-1}$.
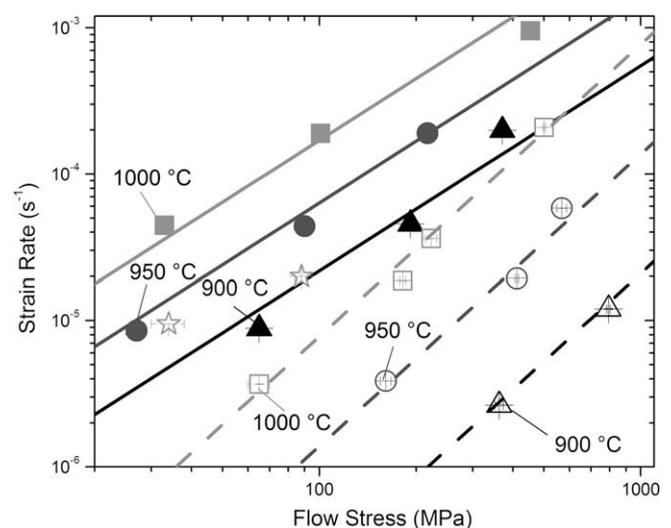
Fig. 6. Double-logarithm plot of compressive strain rate vs. flow stress for 900, 950 and 1000 °C, with best-fit lines determined from Eq. (1) for specimens A (data from Fig. 4 as filled symbols, best-fit lines are continuous) and B (data from Fig. 5 as open symbols, best-fit lines are dashed). The two tensile flow tests at 1000 °C are shown with open star symbols. Error bars correspond to one standard deviation.

mation of -89.5 kJ mol^{-1} [50]. With this melting point, the 1173–1273 K creep temperatures used here for MgB_2 corresponds to $T/T_m \sim 0.51$–0.55, which are at the lower range for diffusional creep of fine-grained ceramics [38].

Specimens of sample B have higher flow stresses, stress exponent ($n = 2.0$) and creep activation energy ($Q = 447$ kJ mol^{-1}) than specimens of sample A. These trends are consistent with a composite strengthening effect [52,53] provided by the increased content of more creep-resistant MgB_4. It can thus be expected that lowering the MgB_4 fraction will produce lower flow stresses and higher ductilities (due to a reduced stress exponent), while also increasing the superconducting critical current density of MgB_2. The MgB_4 phases are too coarse to contribute to stabilization of the fine MgB_2 grain size needed for diffusional creep, but the finer MgO particles may well be needed for this purpose. In fact, the lack of grain growth observed in both specimens following densification and testing at 1000 °C may be due to both the relatively low homologous temperature range and the presence of the fine MgO particles. A stable submicrometer grain size is crucial for the achievement of large-scale plastic deformation at high temperature in most ceramics, and it is probably the case for MgB_2 too, but this point warrants further study. Stable fine grains could alternatively be achieved with additions of SiC or B_4C particles, which also provide significant improvements in superconducting properties by flux pinning [6–8].

3.4. Tensile creep deformation

Tensile deformation at a strain rate of 2×10^{-5} s^{-1} at 1000 °C resulted in yield stresses and flow stresses of $\sim$80 and $\sim$88 MPa for specimens of sample B, as shown in Fig. 4. The 3% tensile strain measured from cross-head displacement was confirmed through measurements of fiducial marks on the specimen gauge length. Tensile deformation performed at half this strain rate resulted in the same ductility of $\sim$3% with yield and flow stresses of $\sim$25 and $\sim$34 MPa, the flow stress being lower by a factor of $\sim$2. The high strain-rate sensitivity (low stress exponent near unity) observed in compression is thus present in tension too, as expected. As compared to compression, however, tensile tests show reductions in both flow stress (Fig. 4) and ductility. This may be due to flaws or cracks that are pre-existing (e.g. produced during machining) or created during deformation (e.g. due to nondeforming MgB_4 and MgO phases). It is likely that tensile deformation of a single-phase MgB_2 wire within a metallic sheath will lead to higher tensile ductilities, due to lack of damage from machining and the protection against necking and surface cracking provided by the ductile sheath. Deformation by hot drawing or hot extrusion of such wires, which is also characterized by a more hydrostatic stress state, is further expected to reduce the propensity for premature tensile fracture.

3.5. Engineering implications

The engineering applications of macroplasticity in MgB_2 at modestly high temperatures (900–1000 °C) include the hot drawing or hot extrusion of PIT wires with dense MgB_2 cores without the use of a complex HIP process and the hot winding of sheathed wires into magnet coils without fracturing their MgB_2 core. Also the increased core density will improve the critical current density and critical field of the wire as compared to the present wires with porous cores. Furthermore, the metallic sheath thickness for the PIT process could be reduced, since the plastic deformation of MgB_2 would not require stresses as high as those needed for crushing hard B or MgB_2 powders near room temperature, as done with the present in situ and ex situ methods. A thinner sheath would further increase the current carrying density of the whole wire.

MgB_2 is one of many isostructural AlB_2-type borides, of which TiB_2 and ZrB_2 currently have the most engineering applications (e.g. as crucible materials and cutting tools) due to their high hardness and melting point. The very high compressive strains demonstrated here for MgB_2 did not require the use of low-melting grain boundary phases, and may be present in TiB_2, ZrB_2 and other AlB_2-type borides (a few of which are given in Fig. 7) at relatively low homologous temperatures T/T_m. A few reports describing modest compressive plasticity at $T/T_m = 0.53$–0.68 exist for: (i) TiB_2 with 2–20 μm grain size exhibiting compressive plastic yielding due to dislocation glide at 1700–2000 °C ($T/T_m = 0.56$–0.65) [22]; (ii) monocrystalline ZrB_2 showing 4.5% compressive yielding at 2125 °C ($T/T_m = 0.68$) at 110 MPa [23]; and (iii) 13% porous polycrystalline ZrB_2 developing 8.5% compressive creep strain at 1600 °C ($T/T_m = 0.53$) at a strain rate of 2×10^{-7} s^{-1} and a stress of 220 MPa [24]. The present results for MgB_2 imply that, for TiB_2, ZrB_2 and other isostructural diborides, reducing
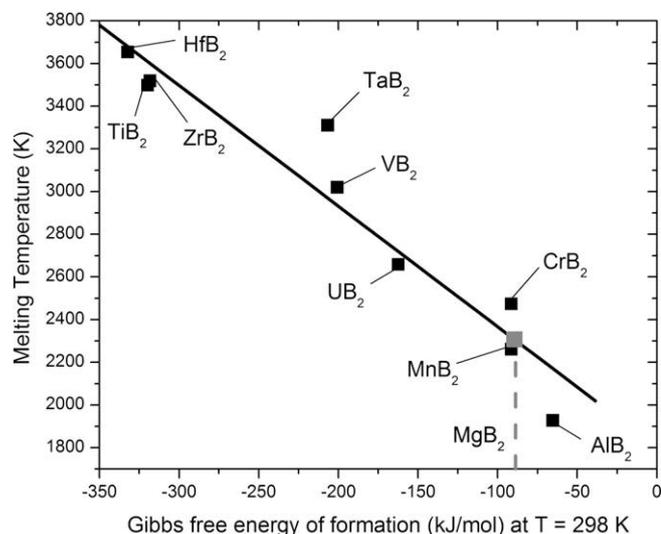

Fig. 7. Plot of melting point vs. Gibbs free energy of formation for nine isostructural AlB_2-type diborides (data from Ref. [50]). The best-fit line predicts a melting point of 2307 K for MgB_2, based on its free energy of formation of -89.5 kJ mol^{-1} [50].

grain size below 1 μm and stabilizing it during deformation may lead to large-scale plasticity at $T/T_{m} \sim 0.5$.

4. Conclusions

The superconducting ceramic MgB_2 can display superplastic compressive strains (true strain of -1.1) at temperatures between 900 and 1000 °C, with grain sizes remaining stable well below 1 μm. The compressive flow stress was measured as a function of deformation rate and temperature, resulting in stress exponents near unity and activation energies near that for interdiffusion, both of which are indicative of a diffusional accommodation mechanism for plastic flow. The commercial MgB_2 powders used here contained ~ 3 vol.% MgO and 5–12 vol.% MgB_4, the presence of which can explain the modest tensile ductility of 3%, which is expected to improve for purer MgB_2 specimens. These results are relevant to the fabrication by hot drawing or hot extrusion of dense MgB_2 wires with metallic sheaths resulting in improved superconducting current density as compared to current wires with porous MgB_2 core, as well as to the possibility for superplastic deformation of other technically important isostructural diborides such as TiB_2 or ZrB_2, allowing shaping and forming of complex objects.

Acknowledgments

References

[1] Nagamatsu J, Nakagawa N, Muranaka T, Zenitani Y, Akimitsu J. Nature 2001;410:63.
[2] Larbalestier DC, Cooley LD, Rikel MO, Polyanskii AA, Jiang J, Patnaik S, et al. Nature 2001;410:186.
[3] Grasso G, Malagoli A, Ferdeghini C, Roncallo S, Braccini V, Siri AS, et al. Appl Phys Lett 2001;79:230.
[4] Glowacki BA, Majoros M, Vickers M, Evetts JE, Shi Y, McDougall I. Supercond Sci Technol 2001;14:193.
[5] Zhou SH, Pan AV, Liu HK, Dou SX. Physica C 2002;382:349.
[6] Yamamoto A, Shimoyama J, Ueda S, Iwayama I, Horii S, Kishio K. Supercond Sci Technol 2005;18:1323.
[7] Dou SX, Soltanian S, Horvat J, Wang XL, Zhou SH, Ionescu M, et al. Appl Phys Lett 2002;81:3419.
[8] Matsumoto A, Kumakura H, Kitaguchi H, Hatakeyama H. Supercond Sci Technol 2003;16:926.
[9] Serquis A, Liao XZ, Zhu YT, Coulter JY, Huang JY, Willis JO, et al. J Appl Phys 2002;92:351.
[10] Kovac P, Husek I, Melisek T. Supercond Sci Technol 2002;15:1340.
[11] Zhang XP, Gao ZS, Wang DL, Yu ZG, Ma YW, Awaji S, et al. Appl Phys Lett 2006;89.
[12] Pan AV, Zhou SH, Liu HK, Don SX. Supercond Sci Technol 2003;16:639.
[13] Chawla N, Chawla KK. Metal matrix composites. New York: Springer-Verlag; 2005.
[14] Shields TC, Kawano K, Holdom D, Abell JS. Supercond Sci Technol 2002;15:202.
[15] Indrakanti SS, Nesterenko VF, Maple MB, Frederick NA, Yuhasz WH, Li S. Phil Mag Lett 2001;81:849.
[16] Serquis A, Civale L, Hammon DL, Liao XZ, Coulter JY, Zhu YT, et al. Appl Phys Lett 2003;82:2847.
[17] Gumbel A, Eckert J, Fuchs G, Nenkov K, Muller KH, Schultz L. Appl Phys Lett 2002;80:2725.
[18] Handstein A, Hinz D, Fuchs G, Muller KH, Nenkov K, Gutfleisch O, et al. J Alloy Compd 2001;329:285.
[19] Jung CU, Park MS, Kang WN, Kim MS, Kim KHP, Lee SY, et al. Appl Phys Lett 2001;78:4157.
[20] Takano Y, Takeya H, Fujii H, Kumakura H, Hatano T, Togano K, et al. Appl Phys Lett 2001;78:2914.
[21] Ramberg JR, Wolfe CF, Williams WS. J Am Ceram Soc 1985;68:C78.
[22] Ramberg JR, Williams WS. J Mater Sci 1987;22:1815.
[23] Haggerty JS, Lee DW. J Am Ceram Soc 1971;54:572.
[24] Melendez-Martinez JJ, Dominguez-Rodriguez A, Monteverde F, Melandri C, de Portu G. J Eur Ceram Soc 2002;22:2543.
[25] Clark JB, Hopple GB, Wright RN. Metall Mater Trans A 1983;14:889.
[26] Eisenstatt LR, Wright RN. Metall Mater Trans A 1980;11:1131.
[27] Soscia GB, Wright RN. Metall Mater Trans A 1986;17:519.
[28] Lubenets SV, Natsik VD, Fomenko LS. Low Temp Phys 2004;30:345.
[29] Eatough MO, Ginley DS, Morosin B, Venturini EL. Appl Phys Lett 1987;51:367.
[30] Albuquerque J, Harmer M, Chou Y. Acta Mater 2001;49:2277.
[31] Yun J, Chou Y, Harmer M. J Am Ceram Soc 2002;85:1190.
[32] Yun J, Harmer MP, Chou YT. Scripta Metall Mater 1993;29: 267.
[33] Yun J, Harmer MP, Chou YT. J Mater Sci 1995;30:4906.
[34] Routbort JL, Goretta KC, Miller DJ, Kazelas DB, Clauss C, Dominguez-Rodriguez A. J Mater Sci 1992;7:2360.
[35] Routbort LR, Miller DJ, Zamirowski EJ, Goretta KC. Supercond Sci Technol 1993;6:337.
[36] Young ML, DeFouw J, Almer JD, Dunand DC. Acta Mater 2007;55:3467.
[37] Goldacker W, Schlachter SI, Obst B, Eisterer M. Supercond Sci Technol 2004;17:S490.
[38] Nieh TG, Wadsworth J, Sherby OD. Superplasticity in metals and ceramics. Cambridge: Cambridge University Press; 1997.
[39] Nieh TG, Wadsworth J. Acta Mater 1990;38:1121.
[40] Gruffel P, Carry P, Mocellin A. Effects of testing conditions on superplastic creep of alumina doped with Ti and Y. In: Taylor D, editor. Science of Ceramics. Stoke-on-trent, vol. 14. The Institute of Ceramics; 1987. p. 587.
[41] Wakai F, Kodama Y, Sakaguchi S, Nonami T. J Am Ceram Soc 1990;73:457.
[42] Wu X, Chen IW. J Am Ceram Soc 1992;75:2733.
[43] Shinoda Y, Nagano T, Gu H, Wakai F. J Am Ceram Soc 1999;82:2916.
[44] Venkatachari KR, Raj R. J Am Ceram Soc 1986;69:135.
[45] Zhan GD, Mitomo M, Nishimura T, Xie RJ, Sakuma T, Ikuhara Y. J Am Ceram Soc 2000;83:841.
[46] Mitomo M, Kim YW, Hirotsuru H. J Mater Res 1996;11:1601.
[47] DeFouw JD, Dunand DC, Quintana JP. Acta Mater 2008;56: 1680.
[48] DeFouw JD, Dunand DC. Acta Mater 2008;56:5751.
[49] Brutti S, Balducci G, Gigli G, Cicciola A, Manfrinetti P, Palenzona A. J Cryst Growth 2006;289:578.
[50] Chemical Rubber Company. CRC handbook of chemistry and physics. Cleveland (OH): CRC Press; 1977.
[51] Fan ZY, Hinks DG, Newman N, Rowell JM. Appl Phys Lett 2001;79:87.
[52] Daymond MR, Lund C, Bourke MAM, Dunand DC. Metall Mater Trans A 1999;30:2989.
[53] Wakai F, Kato H. Adv Ceram Mater 1988;3:71.